

Hollow-core Fiber with Nested Anti-Resonant Tubes for Low-loss THz Guidance

G.K.M. Hasanuzzaman^{1,*}, Stavros Iezekiel¹, Christos Markos², Md. Selim Habib³

¹*Department of Electrical & Computer Engineering, University of Cyprus, Nicosia 1678, Cyprus.*

²*Department of Photonics Engineering, Technical University of Denmark, DK-2800, Kgs. Lyngby Denmark.*

³*The College of Optics and Photonics, University of Central Florida, USA.*

*Corresponding author: ghasan01@ucy.ac.cy

Abstract: A hollow-core fiber with nested anti-resonant node-free cladding tubes suitable for broadband THz guidance with low transmission losses is proposed. It is shown that the tube separation and tube thickness of the inner elements have a significant effect on the confinement loss and effective material loss of these fibers in the THz band. Using TOPAS copolymer, the proposed fiber was optimized for operation at 1 THz and it is predicted from numerical simulations that loss can be reduced to as low as 0.05 dB/m with a 0.6 THz wide dispersion flattened bandwidth.

Keywords: Fiber design and fabrication, Dispersion, Fiber properties, THz fiber.

I. Introduction

One of the keys to the continued growth of terahertz (THz) technology is the development of low loss waveguides, and in particular hollow-core (HC) fibers in which most of the power is guided in the air [1]. Air guidance results in low absorption in the THz spectral range [2,3] while the light is strongly confined in the core of the fiber. In particular, relatively low loss waveguides based on polymers such as PMMA[4], Teflon [5], HDPE [6], Zeonex [7] and Topas [3] have been investigated for use in the 1 THz region. Using these materials, various THz waveguides have been reported, including hollow core fibers [5,6], subwavelength fiber [8], porous-core fibers [9–12], and dielectric tube waveguide [13].

In porous-core (PC) fibers both the core and cladding consist of air-hole microstructures; these fibers have been investigated for low-loss THz waveguiding with high birefringence and low waveguide dispersion [14]. Guiding in a PC fiber can be based either on total internal reflection (TIR) or photonic band gaps (PBG) depending on the air density in the air-hole micro-structured core [15]. PC-PBG fibers provide lower effective material loss (effective material loss is the product of bulk material loss and fraction of power in the background material) than PC-TIR fibers [3]. However, limited transmission bandwidth, strong overlap of the core modes with the surrounding cladding and relatively high group velocity dispersion (especially at the band-gap edges) are major limitations of PC-PBG fibers [15,16].

Hollow core (HC) fibers can be categorized into two types: (i) photonic band gap fiber (HC-PBG) which guides light via the photonic band gap effect. In common with PC-PBG fibers, HC-PBG fibers suffer from limited transmission bandwidth. (ii) Anti-resonant HC fiber (also known as inhibited-coupling HC fiber) in which the guiding mechanism is based on the combination of an anti-resonant effect and inhibited coupling between the core and the cladding modes [17,18].

Hollow core anti-resonant (HC-AR) fibers consisting of a single layer or multiple layers of cladding tubes are of particular interest because these fibers offer much broader transmission bandwidth (more than an octave) and low light-dielectric overlap [19] compared to HC-PBG fibers. The key property of HC-AR fibers is that they exhibit a sequence of narrow-bandwidth/high-loss resonant regions and wide-bandwidth/low-loss

anti-resonant regions. In the resonant regions, core modes are phase matched with the cladding modes causing high transmission loss while in the anti-resonant regions, modes are tightly confined in the air core. The spectral position and bandwidth of the resonant and anti-resonant regions depend significantly on the anti-resonant unit tube thickness [20]. More recently, improved HC-AR fibers with nested anti-resonant tubes have been investigated [17] toward low-loss guidance but most importantly low bend loss. The fiber design is a modified form of HC-AR fiber where smaller tubes are nested inside the tubes defining the core, which provide strong light confinement in the core resulting in low confinement (leakage) loss. Moreover, it has been recently shown that a node-free arrangement in which the cladding tubes are non-touching could be also an alternative to reduce the confinement loss [17,21,22]. This fiber design has been reported in the near infrared and mid infrared spectral regime [17,18][23] but it has never been considered for the THz spectral range.

In this work, we propose for the first time (to the best of our knowledge) the application of a hollow-core nested anti-resonant node-free fiber (HC-NANF)[17][19] for the THz regime (0.5 THz – 1.5 THz). We numerically show that the proposed HC-NANF offers record low effective material loss, broad transmission bandwidth centered at 1 THz, near-zero waveguide dispersion, bend-improved performance and effectively single mode operation while the fiber design relies upon experimentally feasible and realistic fabrication parameters. This is because it has been reported that fiber geometries similar to the ones proposed here can be fabricated using the recent emerging technique of 3D printing [24,25]. Optimizing the design parameters, we predict an effective material loss of 0.05 dB/m; a confinement loss of 3.4×10^{-4} dB/m at 1 THz; a bending loss of 10^{-2} dB/m at 45 cm bending radius; a low-loss transmission band from 0.8 THz to 1.2 THz, for which the total transmission loss is below 0.095 dB/m; and a 0.6 THz flat dispersion band where the dispersion parameter β_2 is less than 0.115993251 ps/THz/cm.

II. Geometry of the proposed design

The geometry of the proposed HC-NANF is shown in Fig. 1. The cladding consists of six circular anti-resonant (AR) tubes in a node-less configuration; each AR tube contains a single circular nested tube. It has been shown that a six-element HC-NANF offers better confinement loss performance than eight or ten elements [17]. In our simulations, we found that a core diameter (D_C) of 3 mm and outer capillary external diameter (d_o) of 2.6 mm gives confinement loss of the order 10^{-4} dB/m, which is low enough for THz guidance [10]. Other design parameters (wall thickness t and tube separation z) were chosen to ensure the anti-resonant first transmission window has a minimum loss around 1 THz. The value of the external diameter of the inner capillary (d_i) is determined from: $d_i = d_o - z - 2t$.

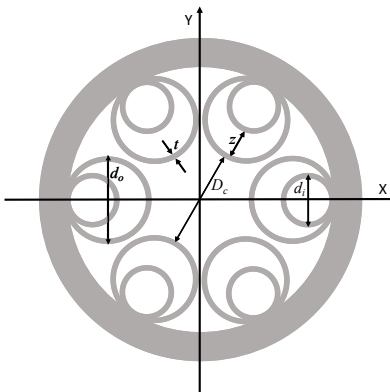


Fig. 1. Geometry of HC-NANF. The fiber has a core diameter $D_C = 3$ mm, outer capillary diameter, $d_o = 2.6$ mm, tube separation $z = 1$ mm and wall thickness, $t = 0.09$ mm.

Topas has been chosen here as the fiber material due to its promising properties in the THz band, including lower bulk material loss than PMMA and Teflon, and constant refractive index n of 1.5258 in the 0.1 THz - 1.5 THz range [26]. The bulk material loss of Topas (α_{mat}) is considered to be linearly proportional to frequency in the 0.2-1.6 THz range and it can be approximated by: $\alpha_{mat}=0.36(f-0.4)+0.06$, where f is in THz and α_{mat} is in dB/cm [2].

III. Simulation results and discussion

The numerical simulations were performed using a finite-element based *COMSOL* software. To calculate the confinement loss of the proposed fiber, a circular perfectly matched layer (PML) was imposed in the outermost part of the structure. In order to obtain accurate results, both the mesh size and perfectly-matched layer parameters were selected using the methodology in [17]. In THz fiber, the dominant type of loss is material absorption loss (also known as effective material loss) which is then added to the confinement loss to estimate the total transmission loss. The fraction of power (η) confined in different regions such as air or fiber material is used to quantify the overlap between light and the material. Effective material loss (α_{EML}) which is defined as the product of bulk material loss (α_{mat}) and fraction of power in the background material (η_m). The following equations are used to calculate confinement loss, effective material loss and fraction of power confined in material [2] [15].

$$\alpha_{cl} = 8.686 \left(\frac{2\pi f}{c} \right) \text{Im}(n_{eff}) \quad \text{dB/m.} \quad (1)$$

$$\alpha_{EML} = \sqrt{\frac{\epsilon_0}{\mu_0}} \frac{\int_{A_{mat}} n \alpha_{mat} |E|^2 dA}{2 \int_{All} S_z dA} = \alpha_{mat} \eta. \quad (2)$$

$$\eta_x = \frac{\int_x S_z dA}{\int_{all} S_z dA}. \quad (3)$$

In the above equations, ϵ_0 and μ_0 are the permittivity and the permeability of vacuum, respectively. The integration of the numerator in (2) is performed over the solid material region of Topas and the integration of the denominator is carried out over all regions, material regions and the air-holes region because air is considered transparent in the THz frequency band. Here S_z is defined as the Poynting vector in the direction of propagation, which is denoted as $S_z = \text{Re}(\mathbf{E} \times \mathbf{H}^*) \cdot \mathbf{z}$, where \mathbf{E} is the electric field component and \mathbf{H} is the magnetic field component. The fraction of power confined in the background material Topas is given by η_m .

To optimize the design parameter, we investigated the effect of core diameter (D_C) and outer capillary external diameter (d_o) on losses as shown in Fig. 2(a) and 2(b) respectively. As observed from Fig. 2 (a) a relatively larger core diameter (D_C) results in reduced losses. However, a larger core diameter also increases the critical bend radius and overall fiber diameter. Furthermore, the fiber's overall diameter also plays an important role in fiber flexibility. In order to be flexible and compact, the fiber should be as thin as possible. Taking these factors into consideration, from here on we set $D_C = 3$ mm and $d_o = 2.6$ mm where the confinement loss is 3.4307×10^{-04} dB/m, the effective material loss is 0.05 dB/m and the overall fiber diameter is 8.5 mm. The fiber diameter is comparable with the fiber in [27]

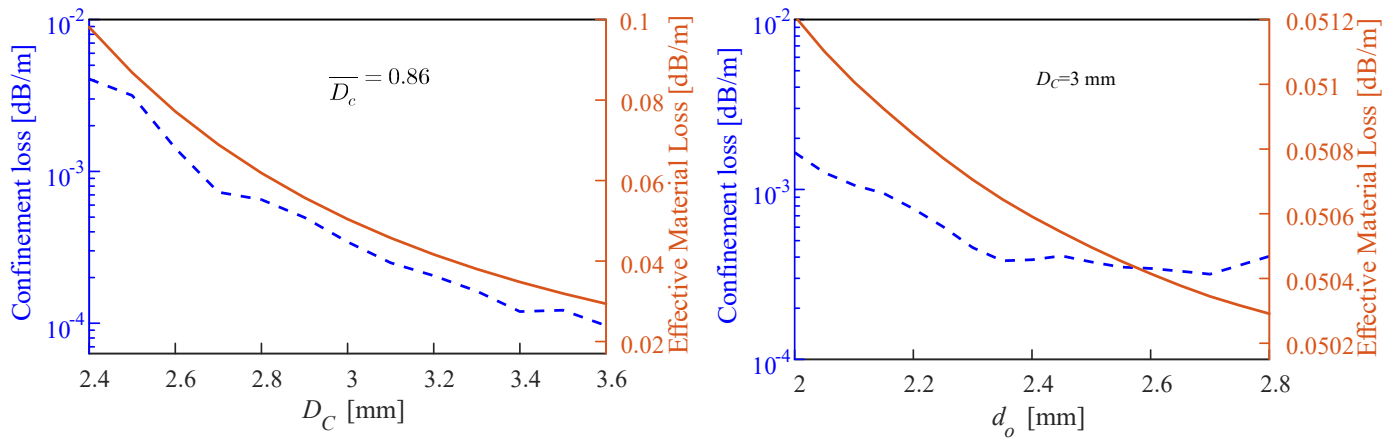


Fig.2: Confinement loss and Effective material loss as a function of (a) Core diameter (D_C) (b) Outer capillary external diameter (d_o).

As discussed in § I, the guiding mechanism of HC-NANF is based on the anti-resonant effect where the anti-resonant tube thickness t determines the position of the high loss resonant windows. The frequency of the first order resonance is given by [17]:

$$f_c \approx \frac{c}{2t\sqrt{n^2 - 1}}. \quad (4)$$

which for $t = \{0.08 \text{ mm}, 0.09 \text{ mm}, 0.10 \text{ mm}, 0.11 \text{ mm}, 0.15 \text{ mm} \text{ and } 0.20 \text{ mm}\}$ and $n = 1.5258$ yields $f_c = \{1.62 \text{ THz}, 1.44 \text{ THz}, 1.30 \text{ THz}, 1.18 \text{ THz}, 0.87 \text{ THz} \text{ and } 0.65 \text{ THz}\}$. These values are in good agreement with the simulated results of Fig.3 where confinement loss is plotted against frequency for different tube thicknesses. The peak in the confinement loss (for $t = 0.10 \text{ mm}$) occurs at around 1.3 THz (Fig.3), which agrees with the analytical results obtained by using (4).

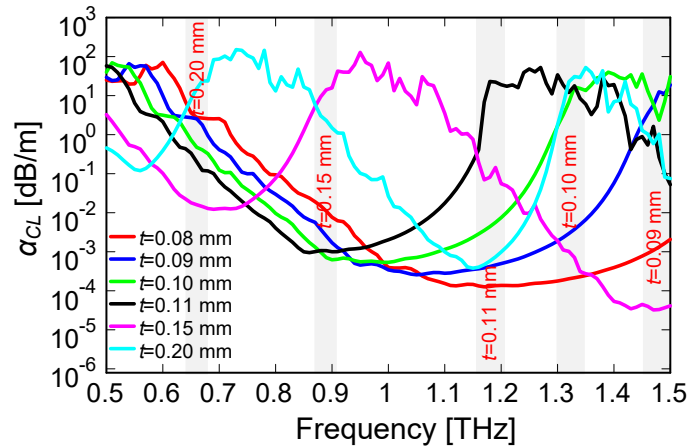


Fig.3: Confinement loss as a function of frequency for different tube thickness t with $D_C = 3 \text{ mm}$, $d_o = 2.6 \text{ mm}$ and $z = 1 \text{ mm}$. The gray shaded regions represent the starting of the resonant bands for corresponding tube thickness.

In THz fiber, the dominant type of loss is material absorption loss (also known as effective material loss). The effective material loss and the total loss of the proposed THz fiber as a function of frequency for different values of wall thickness are shown in Fig. 4 and Fig. 5 respectively.

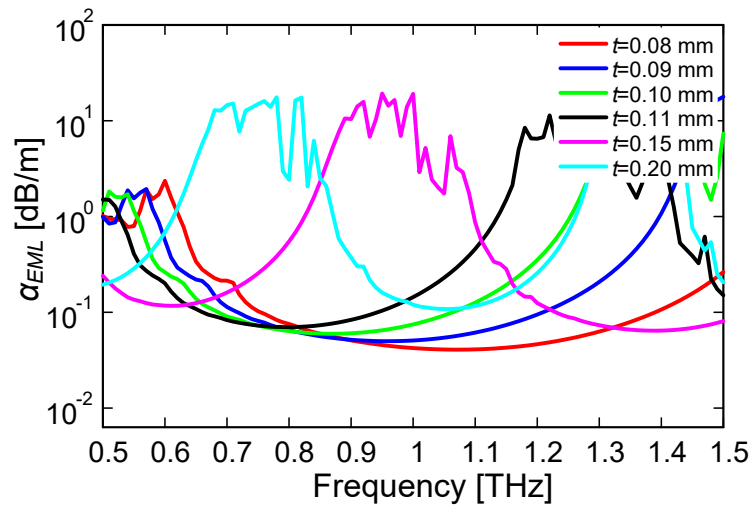


Fig. 4. Effective material loss as a function of frequency for different tube thickness t with $D_C = 3$ mm, $d_o = 2.6$ mm and $z = 1$ mm.

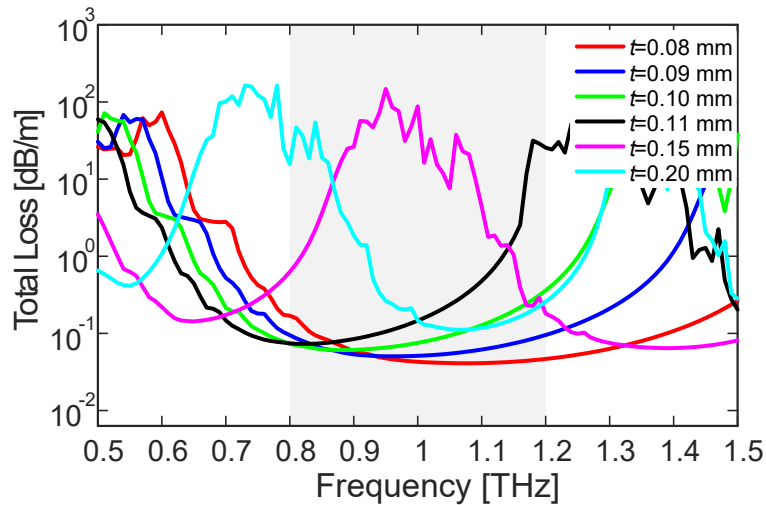


Fig. 5. Total loss as a function of frequency for different values of tube thickness t with $D_C = 3$ mm, $d_o = 2.6$ mm and $z = 1$ mm. The gray shaded region is our band of interest where total loss is minimum for $t = 0.09$ mm (blue line) with low loss characteristics centered at 1 THz.

In the anti-resonant band, α_{EML} dominates the total loss but at the edges of the anti-resonant band confinement loss dominates the total loss. Figure 4 shows that for the higher values of t (e.g. 0.15 mm and 0.20 mm) the resonant band falls around 1 THz resulting in higher transmission losses. The anti-resonant band falls around 1 THz for the relatively lower values of t (e.g. 0.08 mm and 0.09 mm). At 1 THz the confinement loss is lowest for $t = 0.09$ mm (Fig.3) while the effective material loss is lowest for $t = 0.08$ mm (Fig.4). Although the total loss is lowest for $t = 0.08$ mm we chose $t = 0.09$ mm as the preferred value because it provides a wide low-loss band characteristic centered at 1 THz, as shown in the shade-gray region of Fig.5. The calculated transmission loss of the fiber is 0.05 dB/m at 1 THz and it is below 0.095 dB/m within the frequency band 0.8 to 1.2 THz.

Figure 6 shows the loss properties of the fiber as a function of tube separation z at frequency of 1 THz. The confinement loss is high for both high and low values of z , with minimum confinement loss at around 1 mm. However, there is no significant effect of z on effective material loss. This is due to the fact that a very small amount of light interacts with the nested tubes, as shown in the simulated modal field distributions in the insets of Fig. 6. Additionally, the fraction of power in Topas is of the order of 4×10^{-4} . Varying z , it can be

seen that the tube separation has small effect on the numerator in (3) thus indicating negligible influence of z on the α_{EML} .

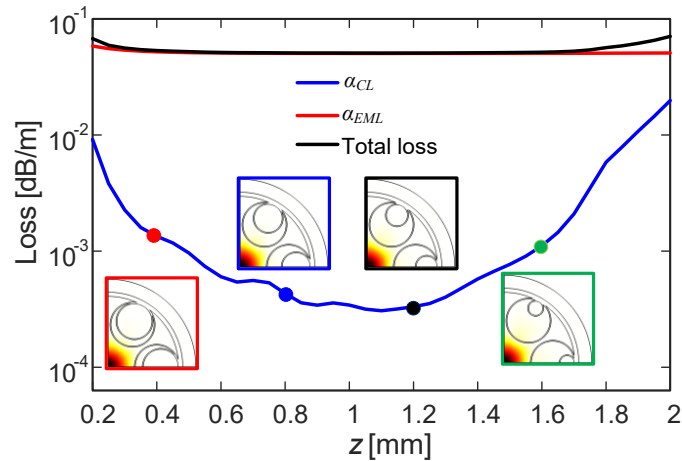


Fig. 6. Effect of changing of tube separation z on loss properties with fixed $D_C = 3$ mm, $d_o = 2.6$ mm, $t = 0.09$ mm and $f = 1$ THz. The color of the frame corresponds to the color of the dots in the plot.

Figure 7 compares the loss performance between the nested HC-AR fiber (with the inner capillary of diameter d_i) and non-nested HC-AR fiber (without the inner capillary of diameter d_i). The non-nested structure provides $\sim 10^2$ times higher confinement loss than the nested structure and thus results in higher total loss. As shown in the contour plot of Fig.7(c) and 7(d), the light is confined strongly for the nested structure. We find that the total loss of the nested HC-AR fiber is 0.05 dB/m whereas the non-nested HC-AR fiber has a loss of 0.1 dB/m at 1 THz for $D_C = 3$ mm, $d_o = 2.6$ mm and $t = 0.09$ mm.

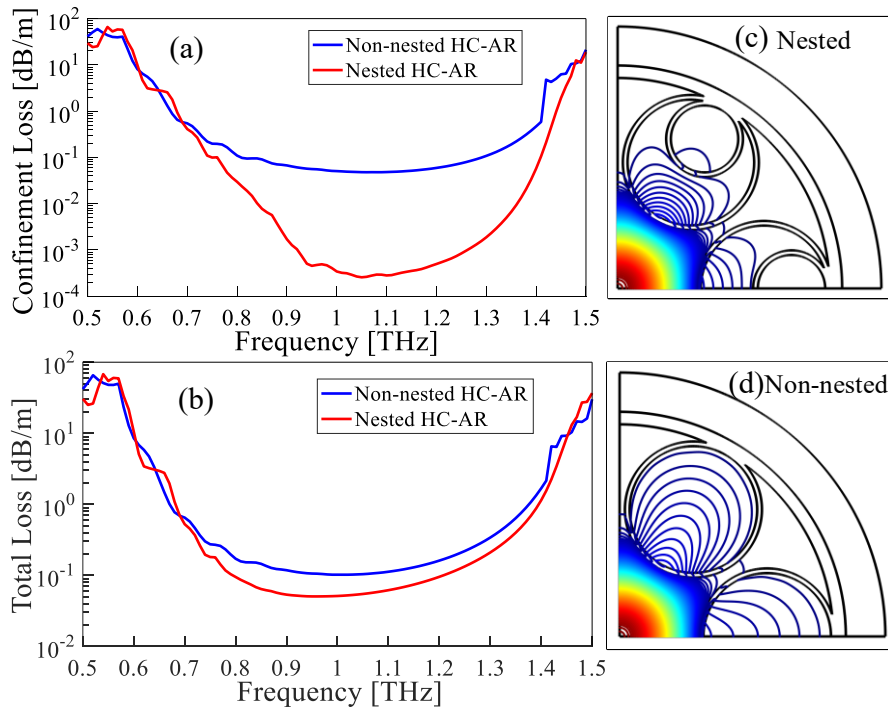


Fig. 7: (a) Confinement loss as a function of frequency (b) Total loss as a function of frequency. Contour plot of electric field pattern of (c) nested structure (d) non-nested structure at 1 THz for $D_C = 3$ mm, $d_o = 2.6$ mm and $t = 0.09$ mm.

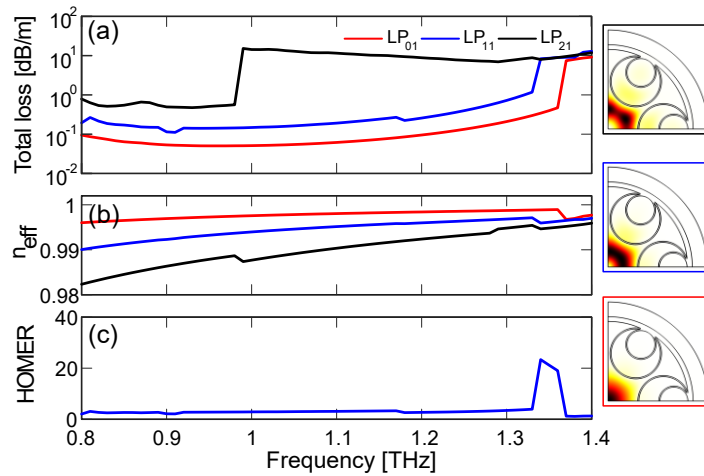


Fig.8. Single mode performance of the proposed fiber as a function of frequency with $D_c = 3$ mm, $d_o = 2.6$ mm, $t = 0.09$ mm and $z = 1$ mm. (a) Total loss (b) Mode index curve (c) HOMER. The color of the frame corresponds to the color of the line in plot (a) and (b).

The higher-order-mode extinction ratio (HOMER), defined as the loss ratio of the higher order mode with lowest loss to the fundamental mode, is used to quantify the degree of higher-order-mode (HOM) suppression [17,28]. The variation of the total loss, effective refractive index of the first three core guided modes (LP₀₁, LP₁₁ and LP₂₁) and HOMER as a function of frequency is shown in Fig. 8. It can be seen from Fig. 8 that at around 1.34 THz the calculated HOMER is 23. This indicates that the losses of higher order modes are at least 23 times higher than the one of the fundamental mode which makes the fiber effectively single-mode at the expense of total loss.

Since the refractive index of Topas is constant between 0.1 THz and 1.5 THz, the material dispersion contribution to the chromatic dispersion can be neglected. We only consider the waveguide dispersion to illustrate the chromatic dispersion profile of the proposed fiber and calculated the group velocity dispersion (β_2) using [15]:

$$\beta_2 = \frac{2}{c} \frac{dn_{eff}}{d\omega} + \frac{\omega}{c} \frac{d^2 n_{eff}}{d\omega^2}. \quad (5)$$

Figure 9 shows that the proposed fiber offers near zero flat dispersion from 0.8 THz to 1.4 THz, where $\beta_2 < 0.115993251$ ps/THz/cm. The variation of β_2 in the flat band is $0.098326176 \pm 0.017667076$ ps/THz/cm. It is noted that the low-loss transmission band shown in Fig. 4 corresponds to a flat dispersion band shown in Fig. 9.

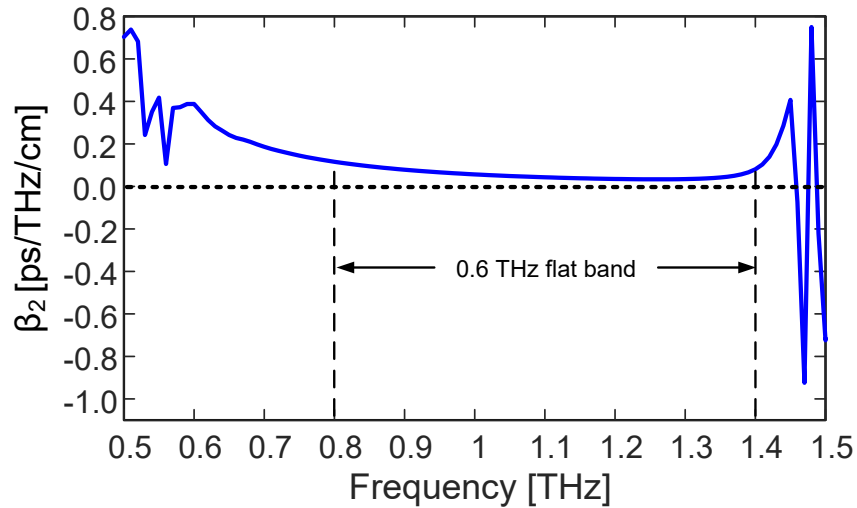


Fig. 9. Dispersion parameter as a function of frequency with $D_C = 3$ mm, $d_o = 2.6$ mm, $t = 0.09$ mm and $z = 1$ mm. The dispersion flattened region coincides with the low loss band shown in Fig. 5 (shaded).

To calculate the bending loss, we used the conformal transformation method to estimate the refractive index profile at bend state. We calculated the effective refractive index distribution after bending using following equation [18]:

$$n_{eq} = n(x, y)e^{(x/R_b)}. \quad (6)$$

where R_b is the bending radius, x is the direction of bending, $n(x, y)$ is the refractive index profile of the straight fiber and n_{eq} is the equivalent refractive index after bending. The bending loss dependency on frequency and normalized bending radius with the optimum design parameters are illustrated in Fig. 10 and Fig. 11 considering bending direction towards the x direction. The coupling effect of this type of fiber is sensitive to structural parameters [29] and we observe a peak in bending loss after the first minima as shown in Fig. 10 and Fig. 11. The peak in the bending loss profile can be predicted analytically from the structural parameters using the following equation for critical bending radius [29]:

$$R_b^{cr} = 1.71 \frac{D_c^3}{\lambda^2} \frac{(d_i/D_c)^2}{1 - (d_i/D_c)}. \quad (7)$$

For our design parameters, we obtain a critical bending radius of 17 cm by using (7). The difference between the analytically and the numerically calculated critical bending radius is due to the approximations used in deriving equation (7) [29]. A bending loss of less than 10^{-2} dB/m is obtained when the bend radius is more than 45 cm.

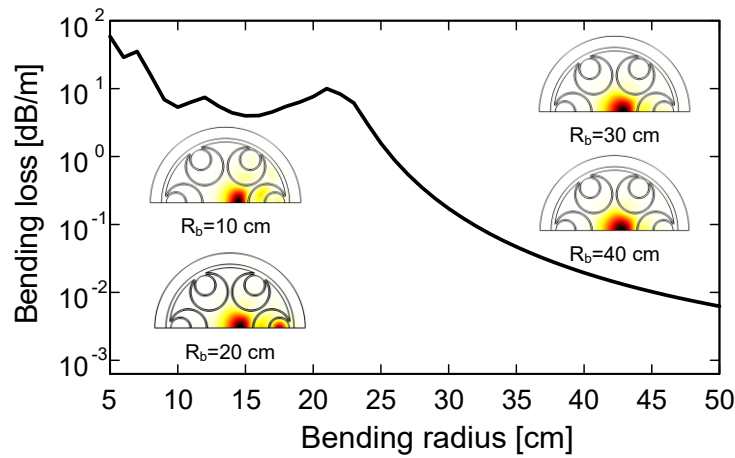


Fig. 10. Calculated bending loss as a function of bending radius at $f = 1$ THz with $D_c = 3$ mm, $d_o = 2.6$ mm, $t = 0.09$ mm and $z = 1$ mm. A peak in bending loss is observed at $R_b \sim 21$ cm.

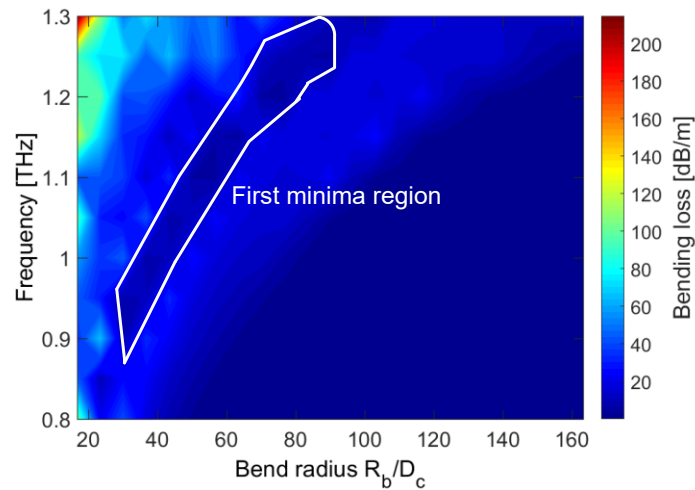


Fig. 11. Calculated bending loss as a function of frequency and normalized bending radius with $D_c = 3$ mm, $d_o = 2.6$ mm, $t = 0.09$ mm and $z = 1$ mm.

Table I summarizes and directly compares recently reported THz fibers operating around 1 THz (including the proposed HC-NANF structure in this work) in terms of structural parameters, guiding mechanisms and effective material loss. Based on previous reports it is evident that the proposed HC-NANF is one of the potential candidates for ultra-low loss, broadband THz wave guiding. Moreover, the HC-NANF proposed here typically requires the stacking of significantly fewer capillaries (in this case 12), as opposed to HC-PBG fibers (the fiber in [6] requires 60 hexagonally-shaped air holes in the cladding alone) or porous-core fibers ([10] requires 49 air holes in the core alone).

Table I: Recently reported THz fibers operating around 1 THz (PC-TIR: Porous core total internal reflection, PC-PBG: Porous core photonic band gap, HC-PBG: Hollow core photonic band gap, HC-IC: Hollow core inhibited coupling, EML: Effective material loss).

THz Fibers	Structure Core-Cladding	Operating Frequency	Guiding Mechanism	Fiber Material	EML	
					In cm^{-1}	In dB/m
Ref [10]	Octagonal -Octagonal	1 THz	PC-TIR	Topas	0.076	33.0068
Ref [9]	Hexagonal- Hexagonal	1 THz	PC-TIR	Teflon	0.12	52.116
Ref [30]	Circular-Octagonal	1 THz	PC-TIR	Topas	0.056	24.3208
Ref [31]	Hexagonal- Kagome	1 THz	PC-IC	Topas	0.035	15.2005
Ref [3]	Hexagonal-Honey comb	1.05 THz	PC-PBG	Topas	0.046	20
Ref [15]	Hexagonal- Hexagonal	1 THz	PC-PBG	Topas	0.099	43.2
Ref [5]	HC -Triangular lattice	1 THz	HC-IC	Teflon	0.01	4.343
Ref [6]	HC-Triangular lattice	0.95 THz	HC-PBG	HDPE	0.0015	0.66
Ref [4]	HC -Kagome	1 THz	HC-IC	PMMA	0.4	173.72
Proposed fiber	HC -Nested tube lattice	1 THz	HC-IC	Topas	0.00011	0.05

IV. Conclusions

In conclusion, we have proposed an experimentally feasible HC-AR fiber in the THz regime and thoroughly investigated the effect of nested anti-resonant elements on losses and the modal properties. By engineering the design parameters in such a way as to maintain the experimental feasibility of the design, we obtain low effective material loss of 0.05 dB/m at $f=1$ THz, 0.4 THz wide low loss transmission window and 0.6 THz wide dispersion flattened band.

V. Acknowledgement

This project has received funding from the European Union's Horizon 2020 research and innovation programme under the Marie Skłodowska-Curie grant agreement No. 642355. Christos Markos has received funding from Det Frie Forskningsråd (DFF) (4184-00359B).

References:

- [1] C. Markos, J.C. Travers, A. Abdolvand, B.J. Eggleton, O. Bang, Hybrid photonic-crystal fiber, *Rev. Mod. Phys.* 89 (2017) 45003. doi:10.1103/RevModPhys.89.045003.
- [2] N. Chen, J. Liang, L. Ren, High-birefringence, low-loss porous fiber for single-mode terahertz-wave guidance, *Appl. Opt.* 52 (2013) 5297–5302. doi:10.1364/AO.52.005297.
- [3] K. Nielsen, H.K. Rasmussen, P.U. Jepsen, O. Bang, Porous-core honeycomb bandgap THz fiber, *Opt. Lett.* 36 (2011) 666. doi:10.1364/OL.36.000666.
- [4] J. Anthony, R. Leonhardt, S.G. Leon-Saval, A. Argyros, THz propagation in kagome hollow-core microstructured fibers, *Opt. Express.* 19 (2011) 18470. doi:10.1364/OE.19.018470.
- [5] J.-Y. Lu, C.-P. Yu, H.-C. Chang, H.-W. Chen, Y.-T. Li, C.-L. Pan, C.-K. Sun, Terahertz air-core microstructure fiber, *Appl. Phys. Lett.* 92 (2008) 64105. doi:10.1063/1.2839576.
- [6] L. Vincetti, Hollow Core Photonic Band Gap Fibre For THz Applications, *Microw. Opt. Technol. Lett.* 51 (2009) 1711–1714.

- [7] J. Anthony, R. Leonhardt, A. Argyros, M.C.J. Large, Characterization of a microstructured Zeonex terahertz fiber, *J. Opt. Soc. Am. B.* 28 (2011) 1013–1018. doi:10.1364/JOSAB.28.001013.
- [8] A. Hassani, A. Dupuis, M. Skorobogatiy, Low loss porous terahertz fibers containing multiple subwavelength holes, *Appl. Phys. Lett.* 92 (2008). doi:10.1063/1.2840164.
- [9] M. Uthman, B.M.A. Rahman, N. Kejalakshmy, A. Agrawal, K.T. V Grattan, Design and characterization of low-loss porous-core photonic crystal fiber, *IEEE Photonics J.* 4 (2012) 2315–2325. doi:10.1109/JPHOT.2012.2231939.
- [10] S.F. Kaijage, Z. Ouyang, X. Jin, Porous-core photonic crystal fiber for low loss terahertz wave guiding, *IEEE Photonics Technol. Lett.* 25 (2013) 1454–1457. doi:10.1109/LPT.2013.2266412.
- [11] R. Islam, M.S. Habib, G.K.M. Hasanuzzaman, S. Rana, M.A. Sadath, C. Markos, A Novel Low-Loss Diamond-Core Porous Fiber for Polarization Maintaining Terahertz Transmission, *IEEE Photonics Technol. Lett.* 28 (2016) 1537–1540. doi:10.1109/LPT.2016.2550205.
- [12] H. Bao, K. Nielsen, H.K. Rasmussen, P.U. Jepsen, O. Bang, Fabrication and characterization of porous-core honeycomb bandgap THz fibers., *Opt. Express.* 20 (2012) 29507–17. doi:10.1364/OE.20.029507.
- [13] H. Bao, K. Nielsen, O. Bang, P.U. Jepsen, Dielectric tube waveguides with absorptive cladding for broadband, low-dispersion and low loss THz guiding, *Sci. Rep.* 5 (2015) 7620. doi:10.1038/srep07620.
- [14] R. Islam, M.S. Habib, G.K.M.K.M. Hasanuzzaman, S. Rana, M.A. Sadath, M. Selim Habib, G.K.M.K.M. Hasanuzzaman, S. Rana, M. Anwar Sadath, Novel porous fiber based on dual-asymmetry for low-loss polarization maintaining THz wave guidance, *Opt. Lett.* 41 (2016) 440–443. doi:10.1364/OL.41.000440.
- [15] J. Liang, L. Ren, N. Chen, C. Zhou, Broadband, low-loss, dispersion flattened porous-core photonic bandgap fiber for terahertz (THz)-wave propagation, *Opt. Commun.* 295 (2013) 257–261. doi:10.1016/j.optcom.2013.01.010.
- [16] F. Benabid, P.J. Roberts, Linear and nonlinear optical properties of hollow core photonic crystal fiber, *J. Mod. Opt.* 58 (2011) 87–124. doi:10.1080/09500340.2010.543706.
- [17] F. Poletti, Nested antiresonant nodeless hollow core fiber, *Opt. Express.* 22 (2014) 23807. doi:10.1364/OE.22.023807.
- [18] M.S. Habib, O. Bang, M. Bache, Low-loss hollow-core silica fibers with adjacent nested anti-resonant tubes, *Opt. Express.* 23 (2015) 17394. doi:10.1364/OE.23.017394.
- [19] W. Belardi, J.C. Knight, Hollow antiresonant fibers with reduced attenuation, *Opt. Lett.* 39 (2014) 1853. doi:10.1364/OL.39.001853.
- [20] L. Vincetti, V. Setti, M. Zoboli, Terahertz tube lattice fibers with octagonal symmetry, *IEEE Photonics Technol. Lett.* 22 (2010) 972–974. doi:10.1109/LPT.2010.2048426.
- [21] M.S. Habib, O. Bang, M. Bache, Low-loss single-mode hollow-core fiber with anisotropic anti-resonant elements, *Opt. Express.* 24 (2016) 8429. doi:10.1364/OE.24.008429.
- [22] A. Van Newkirk, J.E. Antonio-Lopez, J. Anderson, R. Alvarez-Aguirre, Z.S. Eznaveh, G. Lopez-Galmiche, R. Amezcua-Correa, A. Schülzgen, Modal analysis of antiresonant hollow core fibers using S^2 imaging, *Opt. Lett.* 41 (2016) 3277. doi:10.1364/OL.41.003277.
- [23] M. Selim Habib, C. Markos, O. Bang, M. Bache, Soliton-plasma nonlinear dynamics in mid-IR gas-filled hollow-core fibers, *Opt. Lett.* 42 (2017) 2232. doi:10.1364/OL.42.002232.
- [24] A.L.S. Cruz, V.A. Serrão, C.L. Barbosa, M.A.R. Franco, C.M.B. Cordeiro, A. Argyros, X. Tang, 3D printed hollow core fiber with negative curvature for terahertz applications, *J. Microwaves, Optoelectron. Electromagn. Appl.* 14 (2015) SI45-SI53.
- [25] J. Canning, M.A. Hossain, C. Han, L. Chartier, K. Cook, T. Athanaze, Drawing optical fibers from three-dimensional printers, *Opt. Lett.* 41 (2016) 5551. doi:10.1364/OL.41.005551.
- [26] K. Nielsen, H.K. Rasmussen, A.J. Adam, P.C. Planken, O. Bang, P.U. Jepsen, Bendable, low-loss Topas fibers for the terahertz frequency range, *Opt. Express.* 17 (2009) 8592. doi:10.1364/OE.17.008592.
- [27] A. Setti, V. Vincetti, L. Argyros, Flexible tube lattice fibers for terahertz applications, *Opt. Express.* 21 (2013) 3388–3399. doi:10.1016/j.yofte.2012.09.008.
- [28] P. Uebel, M.C. Günendi, M.H. Frosz, G. Ahmed, N.N. Edavalath, J.-M. Ménard, P.S.J. Russell, Broadband robustly single-mode hollow-core PCF by resonant filtering of higher-order modes, *Opt. Lett.* 41 (2016) 1961. doi:10.1364/OL.41.001961.
- [29] M.H. Frosz, P. Roth, M.C. Günendi, P.S.J. Russell, Analytical formulation for the bend loss in single-ring hollow-core photonic crystal fibers, *Photonics Res.* 5 (2017) 88. doi:10.1364/PRJ.5.000088.
- [30] M.I. Hasan, S.M.A. Razzak, G.K.M. Hasanuzzaman, M.S. Habib, Ultra-low material loss and dispersion flattened fiber for THz transmission, *IEEE Photonics Technol. Lett.* 26 (2014) 2372–2375. doi:10.1109/LPT.2014.2356492.
- [31] G.K.M. Hasanuzzaman, M. Selim Habib, S.M. Abdur Razzak, M.A. Hossain, Y. Namihira, Low loss single-mode porous-core kagome photonic crystal fiber for THz wave guidance, *J. Light. Technol.* 33 (2015) 4027–4031. doi:10.1109/JLT.2015.2459232.

